# Modeling and Analysis of Vias in Multilayered Integrated Circuits

Qizheng Gu, Y. Eric Yang, *Member, IEEE,* and M. Ali Tassoudji, *Student Member, IEEE*

***Abstract*—A method for modeling and analyzing vias in multilayered integrated circuits is presented. The model of via structures is constructed based upon microwave network theory. The whole via structure is divided into cascaded subnetworks, including a vertical via passing through different layers and transitions from the microstrip line and/or striplines to the vertical via. The parameters of each subnetwork are obtained from electromagnetic field analysis. Numerical results in the frequency domain and the time domain are presented. Validation of the model has been carried out by both measurements and the FDTD modeling. Comparison to the measurements shows good agreement in the frequency range in which the components of experimental model are within specification, and the time domain simulation results also match well with the FDTD results.**

## I. Introduction

IN ORDER to provide shorter interconnections between different components of a high-performance computer system, modern integrated circuits have incorporated multilayer structures. The interconnects in a multilayer package include not only conventional planar striplines and microstriplines, but vertical transmission lines or so-called vias as well. For example, in the Thermal Conduction Module (TCM) for IBM 3081 and 3090 series computers, the number of vias is rather significant compared to the number of planar interconnects. Therefore, the study of signal propagation properties on vias is indispensable to the understanding of the performance of multilayer integrated circuits.

Unlike striplines and microstriplines, vias do not have parallel ground planes to support well-guided electromagnetic waves. They usually pass through small holes in ground (or reference) planes between individual layers in integrated circuits. The two ends of the via perpendicularly contact the conducting strip of the signal lines in different layers as shown in Fig. 1(a). Therefore, signal distortion is likely to occur when propagating through vias and through the transitions from vias to horizontal signal lines. In the past, vias in printed circuit boards have been analyzed using lumped element circuit models. In [1], the partial electric element circuit (PEEC) model developed by Ruehli [2] was applied to find the inductance of a short flat via connecting two striplines. More recently, integral-equation formulations for quasi-static analysis of various via geometries have been developed [3], [4]. Others [5], [6] use empirical formulas to construct equivalent circuits, which may include transmission line elements. Most of the formulas are only effective at low frequencies. They provide simple and accurate predictions when the lengths of the vias are relatively short and the operating speed is low. For the analysis of high-performance integrated circuit packages, it is desirable to have a comprehensive circuit model that can handle shorter signal pulse duration and rise time, and at the same time remain as simple as these empirical formulas.

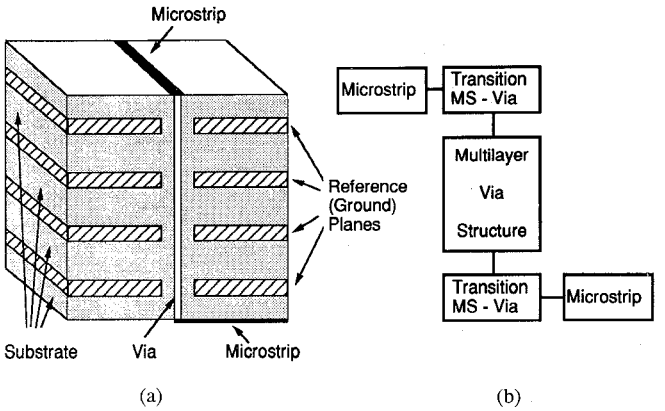


Fig. 1. Configuration and constitution of via structure.

In this paper we will develop an equivalent network model (NW model) for the via structure. The network is constructed from several subnetwork elements corresponding to different parts of the via structure connected in cascade. The parameters of the subnetworks are obtained by electromagnetic analysis based on the geometrical layout of each part. By dividing the structure into subnetworks, we have the flexibility in dealing with modification of circuit geometry. If part of the via structure is changed, only the subnetworks related to the varied section have to be modified.

Section II of this paper will describe the groundwork for constructing an equivalent network of via structures. A general three-dimensional via structure can be decomposed into planar transmission line segments such as microstriplines and/or stripline segments, vertical via and transitions between the planar lines and the vertical via. The analysis of the vertical via will be emphasized in this paper. The equivalent network of the vertical segment and the corresponding network parameters obtained from a magnetic frill model are discussed in detail in Section III. Based on the analytical formulas developed in Section III, transmission and reflection properties of a single layer via and multilayer vias are analyzed. The

Manuscript received February 18, 1992; revised May 29, 1992. This work was supported by ONR Grant N00014–90–J-1002, Joint Service Electronics Program Contract DAAL03–92–C-0001, and Digital Equipment Corporation.

The authors are with the Department of Electrical Engineering and Computer Science and Research Laboratory of Electronics, Massachusetts Institute of Technology, Cambridge, MA 02139.

IEEE Log Number 9204473.

results are presented in Section IV. In order to verify these results, measurements have been performed, and the results are presented in that section. In addition, calculations using the finite-difference time-domain (FDTD) numerical method are made for comparison. The transition from transmission line to vertical via is addressed in Section V. In Section VI, the propagation characteristics of the entire via structure is described in the frequency and time domains.

## II. Via Structure Modeling as Equivalent Networks

The via structure shown in Fig. 1(a) consists of a multilayer substrate with embedded ground planes and microstriplines on the top and bottom layers connected through the vertical via, which is a cylindrical conductor passing through circular holes in the ground planes. This via structure can be decomposed into subsections. These are the microstriplines, transitions, and the vertical via as shown in Fig. 1(b). Each of them can be considered as a two-port network and described by a $2 \times 2$ matrix. As seen in Fig. 1(b), all the two-port subnetworks are connected in cascade, therefore it will be convenient to use the wave transmission matrix $[A_i]$ to represent each of these subnetworks. The matrix expression for the entire via structure is simply the multiplication of the matrices $[A_i]$ [7].

$$[A] = [A_1][A_2]\cdots[A_i]\cdots[A_n]. \tag{1}$$

For example, the via structure in Fig. 1(b) may be characterized by

$$\begin{bmatrix} A_{11} & A_{12} \\ A_{21} & A_{22} \end{bmatrix} = \begin{bmatrix} A_{11T} & A_{12T} \\ A_{21T} & A_{22T} \end{bmatrix}_{MS-V} \begin{bmatrix} A_{11V} & A_{12V} \\ A_{21V} & A_{22V} \end{bmatrix} \begin{bmatrix} A_{11T'} & A_{12T'} \\ A_{21T'} & A_{22T'} \end{bmatrix}_{V-MS} \tag{2}$$

where $[A_T]_{MS-V}$ and $[A_{T'}]_{V-MS}$ are the wave transmission matrices of the transition from the microstripline to via, and vice versa, and $[A_V]$ is the wave transmission matrix of the vertical via.

As will be seen in Section III, the vertical via segment can be further decomposed into subnetworks. The flexibility of such a modeling scheme enables one to implement any variation in the structure by modifying the appropriate subnetwork. This is in contrast with other methods such as full-wave analysis or FDTD which requires the reformulation or recalculation of the overall structure whenever there is a variation in the original structure.

## III. Analysis and Modeling of the Vertical Via

The vertical part of the via structure is isolated in Fig. 2(a). Assuming the ground planes to have finite thickness, we can consider the vertical via to consist of coaxial line segments and radial waveguides. The equivalent network is shown in Fig. 2(b). Since the spacing between the ground planes and the dielectric substrates in each layer are not necessarily the same, every matrix in the network model is not identical. The impedance of each coaxial line segment also varies in accordance with the diameter of the holes in the ground planes and the filling material.

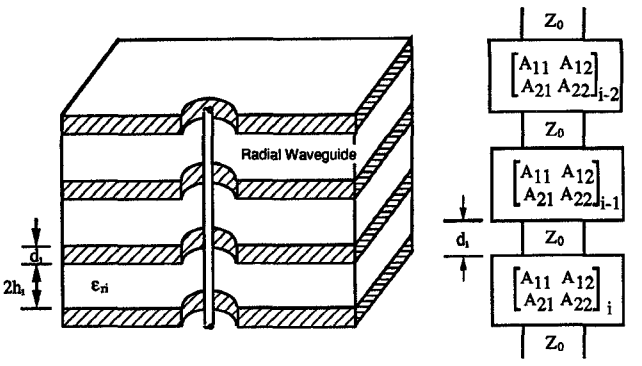


(a) (b)

Fig. 2. Configuration of the vertical via and its equivalent network model.

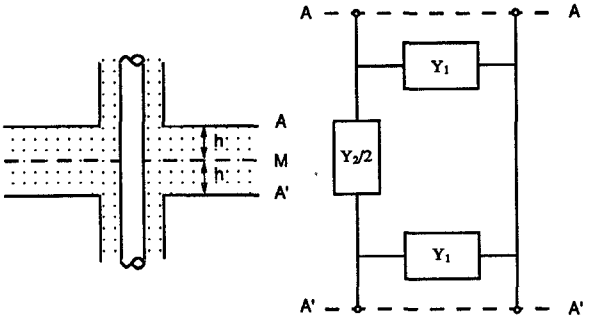


(a) (b)

Fig. 3. Basic unit in multilayer via and its equivalent network.

The network parameters or the elements of the wave transmission matrix $[A_i]$ in the model are obtained based upon the analysis of a basic unit in the multilayer vertical via as shown in Fig. 3(a). In essence, it is a one layer via with coaxial line segments on its ends. To facilitate the analysis, we assume that the coaxial line segments are extended to infinity. The equivalent circuit for the single layer via as shown in Fig. 3(b) is modeled as a $\pi$-type network to exploit the symmetry of the structure. Since the configuration of Fig. 3(a) is symmetric about the mid-plane $M$, the elements in the $\pi$ network can be obtained by analyzing the half structures resulting from placing ideal electric and magnetic walls in turn on the $M$ plane.

In the case of an electric wall placed on the plane $M$, the resulting configuration as shown in Fig. 4(a) is equivalent to a parallel-plate antenna. The corresponding circuit representation is the original $\pi$ network short-circuited in the middle as depicted in Fig. 4(b). The admittance $Y_{sc}$ at plane $A$ observed from the coaxial line side is the same as the input admittance of a parallel-plate antenna. Otto [8] derived the input admittance of the parallel-plate antenna by using a frill model of magnetic current neglecting the effect of TM modes in the coaxial line. We now briefly describe the magnetic frill model to obtain the admittance $Y_{sc}$. Here the radii of the via and the via hole in the ground plane are $a$ and $b$, respectively, and the separation between the ground plane and the electric wall is $h$. Initially, we consider a semi-infinite rod antenna fed by a coaxial line with an inner conductor radius of $a$ (same as

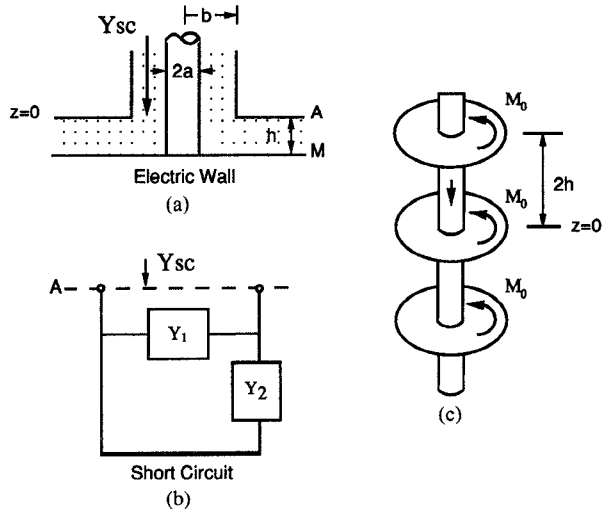


Fig. 4. Configuration for an electric wall placed on plane $M$ and its equivalent and magnetic frill array model. (a) Configuration, (b) equivalent circuit, and (c) magnetic frill array model.

the rod) and an outer radius $b$. By virtue of the equivalence principle, the semi-infinite perfectly conducting rod, which represents the via conductor, is excited by a frill of magnetic current $M_0(z) = M_0\delta(z)$. The frill of magnetic current $M_0$ is located at the aperture where the coaxial line passes through the ground plane and has the form

$$M_0 = \begin{cases} -\dfrac{2V}{r\ln(b/a)}, & a < r < b; \\ 0, & r > b \end{cases} \tag{3}$$

where $V$ is the voltage at the aperture ($z = 0$) on the coaxial line and is usually considered as a known excitation. By using image theory, the structure can be transformed into a periodic array of magnetic frills $M_0$ located at $z = \pm 2mh\,(m = 0, 1, 2, \cdots)$, with the parallel plates removed, as depicted in Fig. 4(c). Mathematically it can be expressed as

$$M_{sc}(z, 2h) = \sum_{m=-\infty}^{+\infty} M_0\delta(z - m(2h)). \tag{4}$$

Using the integral representation of input admittance of infinitely long cylindrical antenna and the concept of periodic frill array, the input admittance of the parallel plate antenna or $Y_{sc}$ can be derived and has the form

$$\begin{aligned} Y_{sc} = &-\frac{2\pi j\sqrt{\epsilon_r}}{\eta_0 \ln\left(\frac{b}{a}\right)}\cot(kh) - \frac{2\pi j\sqrt{\epsilon_r}}{\eta_0 kh\left[\ln\left(\frac{b}{a}\right)\right]^2} \\ &\cdot\left\{\frac{\pi}{2}\frac{H_0^{(2)}(kb)}{H_0^{(2)}(ka)}[J_0(kb)Y_0(ka) - J_0(ka)Y_0(kb)]\right. \\ &-2\sum_{m=1}^{\infty}\frac{1}{q_m^2} \\ &\cdot\left[\frac{K_0(q_m kb)}{K_0(q_m ka)}(I_0(q_m ka)K_0(q_m kb)\right. \\ &\left.\left.-\,I_0(q_m kb)K_0(q_m ka))\right]\right\} \end{aligned} \tag{5}$$

where $k$ is the wavenumber; $\epsilon_r$ is the relative dielectric constant of the filling material; and $J_0, Y_0, I_0, K_0$, and $H_0^{(2)}$ are Bessel functions, modified Bessel functions, and Hankel function of the second kind, respectively. Also,

$$q_m = \sqrt{\left(\frac{m\pi}{kh}\right)^2 - 1}$$

$$\eta_0 = \sqrt{\frac{\mu_0}{\epsilon_0}} \quad \text{the intrinsic impedance of free space.} \tag{6}$$

The form given in (5) is slightly different from that found in [8] because we have used the following identity [9] to simplify one of the series sum:

$$1 - 2\sum_{m=1}^{\infty}\frac{1}{q_m^2} = kh\cot(kh).$$

From the equivalent network Fig. 4(b), it is apparent that the admittance $Y_{sc}$ can be expressed in terms of the elements $Y_1$ and $Y_2$ as

$$Y_{sc} = Y_1 + Y_2. \tag{7}$$

For a magnetic wall replacing the electric wall at the plane $M$, the configuration is shown in Fig. 5(a), and the corresponding equivalent circuit is an open-circuit network [Fig. 5(b)]. The admittance $Y_{oc}$ at $z = 0$ looking from the coaxial side can be determined in a similar manner as for $Y_{sc}$. By the image theory, the equivalent periodic frill array model now consist of alternating magnetic current frills, as shown in Fig. 5(c). The mathematical expression of this frill array is

$$\begin{aligned} M_{oc} &= \sum_{m=-\infty}^{\infty}(-1)^m M_0\delta(z - m(2h)) \\ &= \sum_{l=-\infty}^{\infty} M_0\delta(z - 2l(2h)) \\ &\quad - \sum_{l=-\infty}^{\infty} M_0\delta(z - (2l+1)(2h)) \\ &= 2\sum_{l=-\infty}^{\infty} M_0\delta(z - l(4h)) \\ &\quad - \sum_{m=-\infty}^{\infty} M_0\delta(z - m(2h)). \end{aligned} \tag{8}$$

Comparing (8) to (4), we see that the frill array $M_{oc}(z, 2h)$ can be decomposed into two equivalent short-circuit frill arrays with common excitation voltage at $z = 0$, but spacings of $4h$ and $2h$, respectively. Equation (8), then, can be expressed as

$$M_{oc}(z, 2h) = 2M_{sc}(z, 4h) - M_{sc}(z, 2h). \tag{9}$$

Since the voltage at $z = 0$ is given as a known excitation, the admittance $Y_{oc}$ is directly proportional to the current at $z = 0$ flowing on the inner conductor of the coaxial line. The current at $z = 0$ can be obtained from the equivalent magnetic frill array $M_{oc}$, and hence is the superposition of the currents induced by the equivalent short-circuit frill arrays $2M_{sc}(z, 4h)$

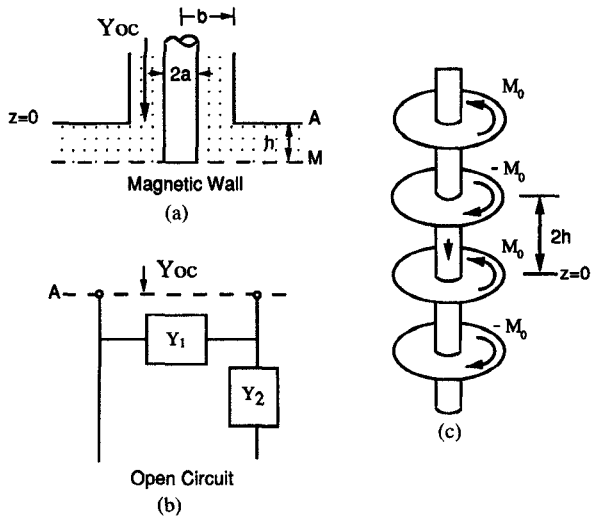


Fig. 5. Configuration for a magnetic wall placed on plane $M$ and its equivalent and magnetic frill array model. (a) Configuration, (b) equivalent circuit, and (c) magnetic frill array model.

and $M_{sc}(z, 2h)$ because of linearity. Thus, $Y_{oc}$ can also be expressed as the superposition of short-circuit admittances

$$Y_{oc} = 2Y'_{sc} - Y_{sc} \tag{10}$$

where $Y_{sc}$ is given by (5) and $Y'_{sc}$ is a short-circuit admittance corresponding to the inner conductor terminated by electric wall with separation $2h$ instead of $h$. $Y'_{sc}$ can further be written in the form of

$$\begin{aligned} Y'_{sc} = &- \frac{2\pi j\sqrt{\epsilon_r}}{\eta_0 \ln\left(\frac{b}{a}\right)} \cot(2kh) \\ &- \frac{\pi j\sqrt{\epsilon_r}}{\eta_0 kh\left[\ln\left(\frac{b}{a}\right)\right]^2}\left\{\frac{\pi}{2}\frac{H_0^{(2)}(kb)}{H_0^{(2)}(ka)}[J_0(kb)Y_0(ka) \right. \\ &- J_0(ka)Y_0(kb)] \\ &- 2\sum_{l=1}^{\infty}\left[\frac{1}{q_{2l-1}^2}\frac{K_0(q_{2l-1}kb)}{K_0(q2l-1ka)}(I_0(q_{2l-1}ka) \right. \\ &\cdot K_0(q_{2l-1}kb) - I_0(q_{2l-1}kb)K_0(q_{2l-1}ka)) \\ &+ \frac{1}{q_{2l}^2}\frac{K_0(q_{2l}kb)}{K_0(q_{2l}ka)}(I_0(q_{2l}ka)K_0(q_{2l}kb)) \\ &\left.\left. - I_0(q_{2l}kb)K_0(q_{2l}ka))\right]\right\}, \end{aligned} \tag{11}$$

where $q_l$ is

$$q_l = \sqrt{\left(\frac{l\pi}{2kh}\right)^2 - 1}.$$

Substituting (5) and (11) into (10), and noting that

$$2\cot(2\theta) = \cot\theta - \tan\theta,$$

we obtain the following form of admittance $Y_{oc}$:

$$\begin{aligned} Y_{oc} = 2Y'_{sc} - Y_{sc} &= \frac{2\pi j\sqrt{\epsilon_r}}{\eta_0 \ln\left(\frac{b}{a}\right)} \tan(kh) \\ &+ \frac{4\pi j\sqrt{\epsilon_r}}{\eta_0 kh\left[\ln\left(\frac{b}{a}\right)\right]^2}\left\{\sum_{n=0}^{\infty}\frac{1}{q_n^2}\frac{K_0(q_nkb)}{K_0(q_nka)} \right. \\ &\left. \cdot [I_0(q_nka)K_0(q_nkb) - I_0(q_nkb)K_0(q_nka)]\right\} \end{aligned} \tag{12}$$

where $q_n$ is

$$q_n = \sqrt{\left(\frac{(2n+1)\pi}{2kh}\right)^2 - 1}. \tag{13}$$

Here we recognize the first terms in (5) and (12) as being the input admittances of the coaxial line TEM mode, and the other terms in these two equations as being related to radial waveguide modes.

It is evident from the equivalent network Fig. 5(b) that $Y_{oc}$ is equal to element $Y_1$, i.e.,

$$Y_1 = Y_{oc}. \tag{14}$$

Substituting (14) into (7), we obtain $Y_2$ to be

$$Y_2 = Y_{sc} - Y_{oc}. \tag{15}$$

From (14), (15), and network theory, the admittance matrix of the $\pi$-network of Fig. 3(b) is

$$\begin{aligned} \begin{bmatrix} Y_{11} & Y_{12} \\ Y_{21} & Y_{22} \end{bmatrix} &= \begin{bmatrix} Y_1 + \frac{Y_2}{2} & -\frac{Y_2}{2} \\ -\frac{Y_2}{2} & Y_1 + \frac{Y_2}{2} \end{bmatrix} \\ &= \begin{bmatrix} \frac{Y_{sc}+Y_{oc}}{2} & -\frac{Y_{sc}-Y_{oc}}{2} \\ -\frac{Y_{sc}-Y_{oc}}{2} & \frac{Y_{sc}+Y_{oc}}{2} \end{bmatrix} \end{aligned} \tag{16}$$

and its corresponding wave transmission matrix is

$$\begin{aligned} \begin{bmatrix} A_{11V}^s & A_{12V}^s \\ A_{21V}^s & A_{22V}^s \end{bmatrix} &= \frac{1}{\overline{Y}_{sc} - \overline{Y}_{oc}} \\ &\begin{bmatrix} 1 + \overline{Y}_{sc} + \overline{Y}_{oc} + \overline{Y}_{sc}\overline{Y}_{oc} & -1 + \overline{Y}_{sc}\overline{Y}_{oc} \\ 1 - \overline{Y}_{sc}\overline{Y}_{oc} & -1 + \overline{Y}_{sc} + \overline{Y}_{oc} - \overline{Y}_{sc}\overline{Y}_{oc} \end{bmatrix} \end{aligned} \tag{17}$$

where

$$\overline{Y}_{sc} = \frac{Y_{sc}}{Y_0} \quad \text{and} \quad \overline{Y}_{oc} = \frac{Y_{oc}}{Y_0} \tag{18}$$

and $Y_0$ is the characteristic admittance of the coaxial line.

The wave transmission matrix in (17) characterizes a single layer vertical via. In the case of an $n$-layer via as depicted in Fig. 2(a), the wave transmission matrix takes the form

$$\begin{aligned} \begin{bmatrix} A_{11V} & A_{12V} \\ A_{21V} & A_{22V} \end{bmatrix} &= \begin{bmatrix} A_{11C} & A_{12C} \\ A_{21C} & A_{22C} \end{bmatrix}_1 \\ &\cdot \prod_{i=1}^{n}\left\{\begin{bmatrix} A_{11V}^s & A_{12V}^s \\ A_{21V}^s & A_{22V}^s \end{bmatrix}_i \begin{bmatrix} A_{11C} & A_{12C} \\ A_{21C} & A_{22C} \end{bmatrix}_{i+1}\right\} \end{aligned} \tag{19}$$

where $[A_V^s]_i$ $(i = 1, 2, \cdots, n)$ have the same form as (17), but the parameters $\overline{Y}_{sc,i}$ and $\overline{Y}_{oc,i}$ depend on the dimensions and properties of layer $i$, and $[A_C]_l$ $(l = 1, 2, \cdots, n+1)$ is the wave transmission matrix of the $l$th segment of the coaxial line

$$[A_C]_l = \begin{bmatrix} e^{j\theta_l} & 0 \\ 0 & e^{-j\theta_l} \end{bmatrix}. \tag{20}$$

In (20), the elements are normalized to the corresponding characteristic impedance of the coaxial line, and $\theta_l$ is the electrical length of the $l$th segment

$$\theta_l = \frac{2\pi}{\lambda_{gl}} d_l \tag{21}$$

where $\lambda_{gl}$ is the guide wavelength in the $l$th coaxial line segment, and $d_l$ is its physical length.

For a uniform vertical via in which the dimensions and filling material of each layer as well as all the segments of the coaxial line are identical, i.e., $\theta_l = \theta$, expression (19) becomes

$$\begin{bmatrix} A_{11V} & A_{12V} \\ A_{21V} & A_{22V} \end{bmatrix} = \begin{bmatrix} e^{j\theta/2} & 0 \\ 0 & e^{-j\theta/2} \end{bmatrix} \cdot \begin{bmatrix} A^s_{11V} e^{j\theta} & A^s_{12V} \\ A^s_{21V} & A^s_{22V} e^{-j\theta} \end{bmatrix}^n \cdot \begin{bmatrix} e^{j\theta/2} & 0 \\ 0 & e^{-j\theta/2} \end{bmatrix}. \tag{22}$$

Once the total transmission matrix $[A_V]$ has been calculated, the reflection coefficient $\Gamma_v$ and the transmission coefficient $T_v$ at the input of the vertical via are as follows:

$$\Gamma_v = S^v_{11} = \frac{A_{21V}}{A_{11V}}, \tag{23}$$

and

$$T_v = S^v_{21} = \frac{1}{A_{11V}}. \tag{24}$$

So far, the analysis has been performed in the frequency domain. The reflected and transmitted time domain waveforms of a pulse signal propagating through the via can be obtained by means of Fourier transform.

## IV. Validation and Application of the Vertical Via Model

The network model of the vertical via portion of the structure presented in the previous section is obtained by neglecting the effect of TM modes in the coaxial line. We further consider the limiting case in which the length of the coaxial line segments in the multilayer via becomes zero. With these assumptions, the NW model has been validated with experimental measurement and the finite-difference time-domain numerical calculation.

We shall begin with the single layer vertical via, fed and terminated by a coaxial line as illustrated in Fig. 3. The dimensions and the filling dielectric material correspond to realistic via structures in integrated circuits and are based on the ease of constructing the experimental model. The radius of the via which equals the inner conductor of the coaxial line is

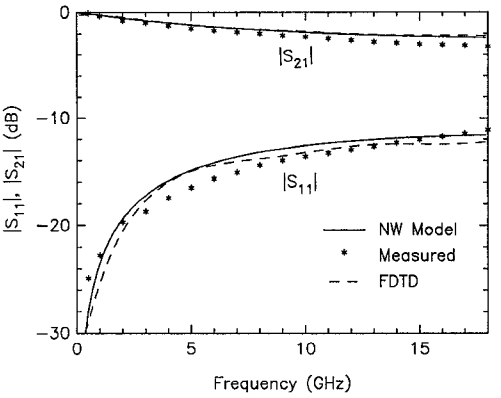


Fig. 6. $|S_{11}|$ and $|S_{21}|$ of the single-layer vertical via.

$a = 0.457$ mm, the radius of the apertures in the ground planes and also the outer radius of the coaxial line is $b = 1.524$ mm, the spacing between two ground planes is $2h = 1.524$ mm, and the relative permittivity $\epsilon_r$ of the filling material is 2.2. Due to the symmetry of the vertical via, its properties can be solely characterized by the reflection coefficient $S^v_{11}$ and the transmission coefficient $S^v_{21}$. The magnitudes of $S^v_{11}$ and $S^v_{21}$, for a single layer vertical via with the above dimensions and filling material, calculated using (5), (12), (17), (23), and (24), are presented in Fig. 6 with solid lines.

An experimental model is built from commercially available products: RT/Duroid 5880 laminate and 141 ISOCORE semirigid cable. The laminate board was cut to a size of 152.4 × 101.6 mm. A through-hole with a diameter of 0.914 mm was made in the middle of the board. Circular pads centered at the through-hole on both sides of the board with diameter of 3.048 mm are etched. A 15-cm-long coaxial cable is used. Its outer conductor and dielectric on half of the cable are extracted. The other half with the inner conductor is passed through the via hole of the board. The outer portion is then placed back on the inner conductor that was extended from the laminate board. The outer conductors of the cable are then soldered to the copper on both sides of the RT/Duroid. SMA connectors are used at the ends of the semirigid cable. Since the performance of the cable and connectors are good up to 18 GHz, the same frequency range is chosen for the measurements. The results for transmission and reflection are shown with asterisks in Fig. 6. A good agreement between the calculated results obtained from the formulas given in Section III and the measurements is observed. In the experiment, the HP 8510B network analyzer system is used to measure the $S$ parameters of the model under test.

For further validation of the NW model, the finite-difference time-domain (FDTD) technique [10] is used to indirectly calculate the reflection and transmission coefficients. A second-order absorbing boundary condition derived by Engquist and Majda [11] is used. In the FDTD calculation, rectangular grids are employed, hence a coaxial line with square cross section is used instead of a circular coaxial line. The inner conductor of the square coaxial line has a 0.914 × 0.914 mm cross section, and the inside dimension of the outer conductor is 2.743 × 2.743 mm. The filling material of the cable has a relative permittivity of 2.1. Using the approxi-

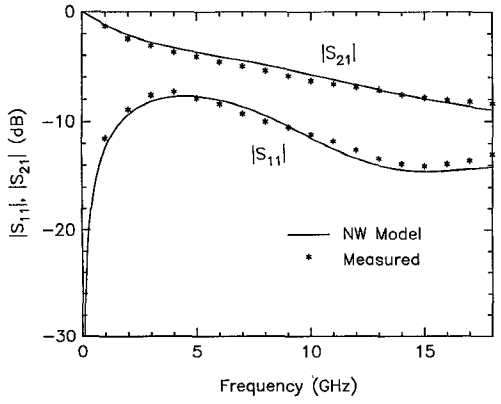


Fig. 7. $|S_{11}|$ and $|S_{21}|$ of 4-layer vertical via.

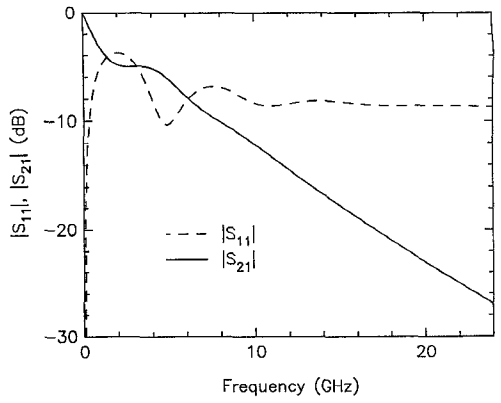


Fig. 8. Frequency responses of $|S_{11}|$ and $|S_{21}|$ for a 10-layer vertical via.

mate formula for the square coaxial line given in [12], the characteristic impedance of this coaxial line is 49.7 Ω. The calculated results are denoted in Fig. 6 by dashed curves. There is good agreement for frequencies above 2 GHz, while at low frequencies the FDTD accuracy decreases because the geometry enclosed by our computational domain becomes comparable to wavelength. It can of course be improved by increasing the number of grids and keeping the same grid size, but this requires more computation time. On the other hand, it is not feasible to increase the grid size to enlarge the geometry, because in our case the grid size is limited by the via dimensions. Techniques such as nonuniform grids and different grid size in different frequency ranges can be used to improve the calculation accuracy and control the computation time. However, compared to the NW model, the required computation times are in general very long. On a DEC Station 3100 computer, the time for calculating the single layer vertical via based on the NW model is less than 1 min, while it takes over 2 hours using FDTD within a domain of a $60 \times 60 \times 60$ grid.

A 4-layer vertical via was also calculated and measured, with each layer having the same dimensions and filling material as the single layer. The results are shown in Fig. 7, where solid curves are obtained from (5), (12), (17), and (22)–(24), and the asterisks represent the measurement data. Once again, the results demonstrate that the calculation from the NW model are in very good agreement with the measurements.

The complexity of the geometry model for numerical approaches increases with the number of layers. In contrast, this vertical via model provides an efficient way of predicting the performance of vertical vias with ten or even more layers just as easy as it would take for one or two layers. As an example, we now consider a multilayer vertical via similar to the IBM 3081 TCM. In this vertical via, the circular via has a radius of $a = 0.0625$ mm and goes through holes of radius $b = 0.1875$ mm in the ground planes. Each layer is composed of ceramic filling with a relative permittivity $\epsilon_r = 10.0$ thickness $2h = 0.6$ mm. Fig. 8 shows the frequency domain transmission and reflection coefficients of a 10-layer structure. It is obvious that reflection is generally high and transmission drops rapidly with respect to frequency. We observe oscillations in the reflection coefficient, which is due to interference of multiple reflections from the junctions. The frequency dependence of

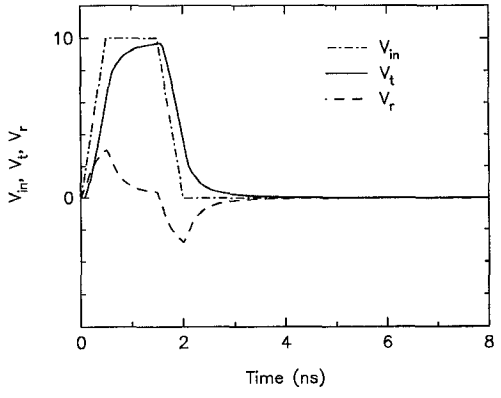


Fig. 9. Time waveforms in the 10-layer vertical via for a trapezoidal pulse input with rise time of 500 ps.

the transmission coefficient has significant impact on how fast the circuit can operate. In Figs. 9 and 10, we compare the time domain responses of a 10-layer vertical via subject to trapezoidal pulses of 1 ns duration with 500 ps and 100 ps rise time, respectively. The relative amplitude of these pulses is 10. Note that at 100 ps rise time, the leading edge of the transmitted waveform, defined as the portion from 10 to 90% of the peak amplitude, suffers significant degradation and virtually loses the sharp edge needed for fast switching further down the interconnecting path. The deterioration of the transmitted signal is also observed when the number of layers increases. Hence, it is clear that the physical configuration, material property, and number of layers of a vertical via can heavily impact the practical limit of how fast the integrated circuit can operate.

## V. Transitions from Transmission Line to Vertical Via

Any three-dimensional integrated circuit employing via structures is bound to encounter the transitions from microstrip or stripline to vertical via. The via structure given in Fig. 1(a) contains two microstrip–via transitions. In other cases, the via structures might contain stripline–via transitions or both types of transitions.

We consider the ground plane to have finite thickness, and the portion of the vertical via passing through the hole in the ground plane as a segment of a coaxial line to be

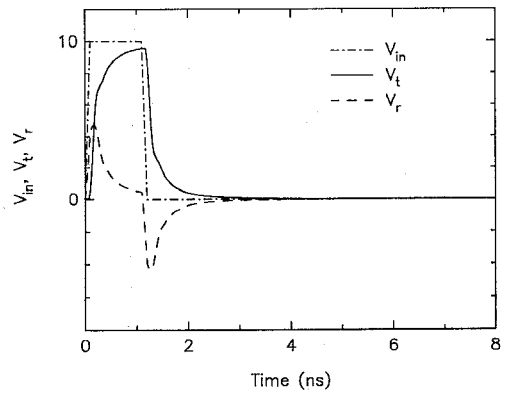


Fig. 10. Time waveforms in the 10-layer vertical via for a trapezoidal pulse input with rise time of 100 ps.

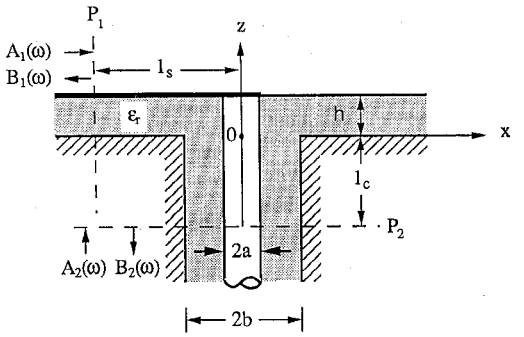


Fig. 11. Configuration of the transition between microstripline and coaxial line.

consistent with the treatment in Section III. The transition is then approximated as a junction between microstripline or stripline and a coaxial line. We shall represent the transitions by two-port networks connected in cascade with the vertical via network. As shown in Fig. 11, reference planes $P_1$ and $P_2$ on the microstrip and coaxial line are respectively chosen to be far enough away from the junction. Thus, the transition can be characterized by a scattering matrix as follows:

$$\begin{bmatrix} \frac{B_1(\omega)}{\sqrt{Z_1}} \\ \frac{B_2(\omega)}{\sqrt{Z_2}} \end{bmatrix} = \begin{bmatrix} S_{11}(\omega) & S_{12}(\omega) \\ S_{21}(\omega) & S_{22}(\omega) \end{bmatrix} \begin{bmatrix} \frac{A_1(\omega)}{\sqrt{Z_1}} \\ \frac{A_2(\omega)}{\sqrt{Z_2}} \end{bmatrix} \tag{25}$$

where $A_i$ and $B_i$ $(i = 1, 2)$ represent the incident and reflected voltage waves, respectively, on the microstrip and the coaxial line, and $Z_i$ $(i = 1, 2)$ are the characteristic impedances of these two lines. The network parameters of the transition can be obtained indirectly from the reflection and transmission coefficients on the microstrip side when the coaxial side is terminated with different loads, such as matched load and short circuit. When the coaxial line is terminated with a load $R_L$ at reference plane $P_2$, the reflection coefficient $\Gamma$ at reference plane $P_1$ on the microstrip is of the form

$$\Gamma(\omega) = \frac{B_1(\omega)}{A_1(\omega)} = S_{11}(\omega) + \frac{S_{12}(\omega)S_{21}(w)\Gamma_L}{1 - S_{22}(\omega)\Gamma_L} \tag{26}$$

and the transmission coefficient $T$ from plane $P_1$ to $P_2$ has the form

$$T(\omega) = \frac{B_2(\omega)/\sqrt{Z_2}}{A_1(\omega)/\sqrt{Z_1}} = S_{21}(\omega)\left(1 + \frac{S_{22}(\omega)\Gamma_L}{1 - S_{22}(\omega)\Gamma_L}\right) \tag{27}$$

where $\Gamma_L$ is the reflection coefficient of the load at plane $P_2$ on the coaxial line, and it has the expression

$$\Gamma_L = \frac{R_L - Z_2}{R_L + Z_2}.$$

The coefficients $\Gamma$ and $\Gamma$ can be numerically determined in the frequency domain through solving a set of coupled integral equations governing the current distribution on the microstrip and the inner conductor of the coaxial line. The coupled integral equations are derived from the analysis of electric field in the transition and boundary conditions [13] in terms of known dyadic Green's function of layered media [14]. The coefficients or the $S$ parameters of the transition can also be obtained by means of the FDTD approach. In this case, however, it is preferable to calculate the $S$ parameters based on (25) and exciting the transition from the microstripline side and the coaxial line side, respectively, while the other end is terminated with a matched load. The reason is that any excitation in a zero- or low-loss system with discontinuities and shorted-circuit terminations will have long time responses resulting from wave bouncing back and forth between the discontinuities and the terminals with slow decays. This will increase the computation time for FDTD solutions. The details of analyzing and modeling the transition are the subject of a forthcoming paper.

In order to integrate the transmission matrix $A_T^o$ of the transition depicted in Fig. 11 to the via structure, it is necessary to shift the reference plane $P_2$ on the coaxial line to the ground plane $(z = 0)$. Here, we assume again that only the TEM mode exists on the coaxial line. Hence, the final transmission matrix of the transition is given as

$$\begin{bmatrix} A_{11T} & A_{12T} \\ A_{21T} & A_{22T} \end{bmatrix} = \begin{bmatrix} A^o_{11T} & A^o_{12T} \\ A^o_{21T} & A^o_{22T} \end{bmatrix} \begin{bmatrix} e^{-j\theta_c} & 0 \\ 0 & e^{j\theta_c} \end{bmatrix} \tag{28}$$

where $\theta_c$ is the electrical length of the distance $l_c$ from the ground plane to the reference plane $P_2$.

In Fig. 12, we present the magnitudes of $S$ parameters calculated from the FDTD approach and also the measurements for a transition between a microstripline and a coaxial line. The dimensions of the transition are $h = 0.751$ mm, width of microstrip $w = 2.135$ mm, $a = 0.475$ mm, $b = 1.524$ mm, and $\epsilon_r = 2.2$. The maximum discrepancy between the computed and the measured results over the frequency range from 45 MHz to 18 GHz is less than 2.1 dB. A higher transmission loss in the experimental model is due to the long lengths of the microstrip and coaxial line which are 6 cm and 16 cm, respectively.

## VI. Simulation Results of Via Structure

To demonstrate the usage of the approaches described in the previous sections, we simulate the entire via structure consisting of two identical transitions and a 4-layer vertical via. The configuration is similar to that given in Fig. 1(a), except that the vertical via part is now of 4 identical layers

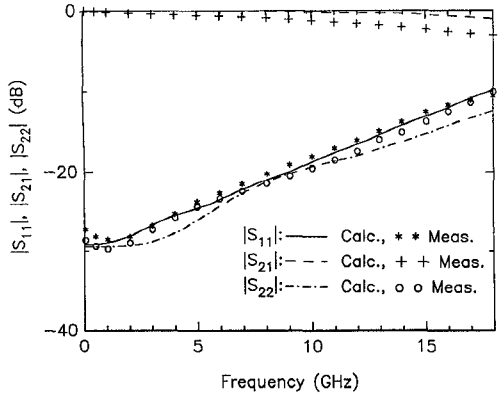


Fig. 12. Magnitudes of $S$ parameters for the transition between microstrip and coaxial line.

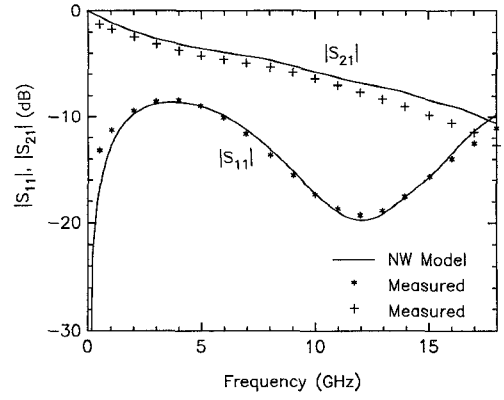


Fig. 13. Magnitudes of $S$ parameters for the 4-layer via structure.

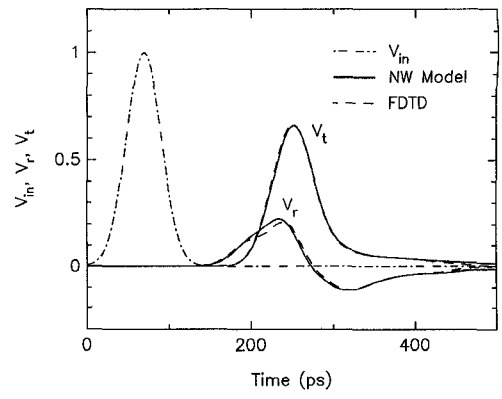


Fig. 14. Time waveforms for 4-layer via structure with a 50 ps Gaussian pulse input.

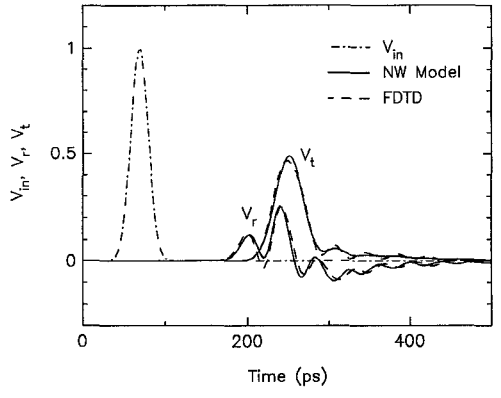


Fig. 15. Time waveforms for 4-layer via structure with a 25 ps Gaussian pulse input.

instead of 3. The dimensions used in this simulation are exactly the same as those given in Sections IV and V. The frequency response of the 4-layer via structure calculated from the NW model is shown with solid lines in Fig. 13. Measurement results are also presented for comparison. Over the range from 1 to 18 GHz, the maximum deviation between calculated and measured $|S_{11}|$ is about 1 dB. The discrepancy in the transmission coefficient $|S_{21}|$ is slightly higher, reaching 2 dB at 18 GHz. This can be accounted for by the material and conductor loss in the experimental model.

We also conducted a time-domain simulation of the 4-layer via structure under Gaussian pulse excitations. The reflected and transmitted waveforms simulated by the NW model when Gaussian pulses with 50 and 25 ps pulse widths (measured at their half amplitude) propagate through the 4-layer via structure are depicted with solid lines in Figs. 14 and 15. In order to verify the simulation in the time domain and in the absence of corresponding experimental measurement, the FDTD approach is applied to simulate the reflected and the transmitted waveforms in the same via structure, and the results are shown as dashed lines in Figs. 14 and 15. It can be seen that the waveforms obtained from the NW model and the FDTD method match very well.

## VII. Conclusions

A modeling method for the via structure has been developed based on the equivalent network approach. The advantages of the new modeling method are its flexibility and short computation time. It is very easy to modify the NW model to accommodate the changes in circuit geometry because we are dealing with individual submatrices corresponding to building blocks of the circuit. By adding, removing, or combining submatrices, we can also create the model for a new via structure. With its advantage of quick solutions and reconfigurability, the network model has the potential of a good engineering design tool.

The frequency range of validity of the via model depends on whether the assumption for deriving the parameters of the equivalent subnetwork fails. It varies with the dimensions and material properties of the via structure being modeled. Smaller via structures generally have a higher frequency limit. In the examples mentioned in this paper, the dimensions of the via structure are quite large, about the order of 1 mm. By comparing the results to those from the FDTD calculation, we found them to be valid up to 25 GHz. They also match very well with measurements.

## Acknowledgment

The authors wish to thank Dr. S. Poh for his careful reading and many helpful suggestions. They would also like to express their gratitude to Dr. D. M. Sheen for providing the FDTD program, as well as B. Meskoob and Y. Huang for their assistance in the measurement.

## REFERENCES


[1] A. Djordjević and T. K. Sarkar, "Computation of inductance of simple vias between two striplines above a ground plane," *IEEE Trans. Microwave Theory Tech.*, vol. MTT-33, pp. 268–269, Mar. 1985.

[2] A. E. Ruehli, "Equivalent circuit models for three-dimensional multiconductor systems," *IEEE Trans. Microwave Theory Tech.*, vol. MTT-22, pp. 216–221, Mar. 1974.

[3] T. Wang, R. F. Harrington, and J. R. Mautz, "Quasi-static analysis of a microstrip via through a hole in a ground plane," *IEEE Trans. Microwave Theory Tech.*, vol. 36, pp. 1008–1013, June 1988.

[4] P. Kok and D. D. Zutter, "Capacitance of a circular symmetric model of a via hole including finite ground plane thickness," *IEEE Trans. Microwave Theory Tech.*, vol. 39, pp. 1229–1234, July 1991.

[5] J. P. Quine, H. F. Webster, H. H. Glascock, and R. O. Carlson, "Characterization of via connections in silicon circuit boards," *IEEE Trans. Microwave Theory Tech.*, vol. 36, pp. 21–27, Jan. 1988.

[6] M. E. Goldfarb and R. A. Pucel, "Modeling via hole grounds in microstrip," *IEEE Microwave Guided Wave Lett.*, vol. 1, pp. 135–137, June 1991.

[7] R. E. Collin, *Field Theory of Guided Waves*. New York: McGraw-Hill, 1960.

[8] D. V. Otto, "The admittance of cylindrical antennas driven from a coaxial line," *Radio Science*, vol. 2, no. 9, pp. 1031–1042, 1967.

[9] M. Abramovitz and I. A. Stegun, *Handbook of Mathematical Functions*. New York: Dover, 1965, p. 75.

[10] K. S. Yee, "Numerical solution of initial boundary value problems involving Maxwell's equations in isotropic media," *IEEE Trans. Antennas Propagat.*, vol. AP-14, no. 5, pp. 302–307, May 1966.

[11] B. Engquist and A. Majda, "Absorbing boundary conditions for the numerical simulation of waves," *Math. of Comp.*, vol. 31, no. 139, pp. 629–651, 1977.

[12] K. H. Lau, "Loss calculations for rectangular coaxial lines," *Proc. Inst. Elec. Eng.*, vol. 135, pt. H, no. 3, pp. 207–209, June 1988.

[13] J. R. Mosig, "Integral equation technique," in *Numerical Techniques for Microwave and Millimeter-Wave Passive Structures*, T. Itoh, Ed. New York: Wiley, 1989.

[14] J. A. Kong, *Electromagnetic Wave Theory*. New York: Wiley, 1990.


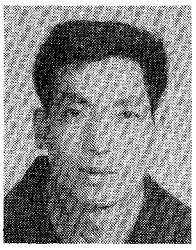

**Qizheng Gu** was born in Jiangsu, China. He graduated from Fudan University, Shangai, China.

He worked on the design and analysis of automatic control systems at Shanghai Designing Institute of Machinary and Electrical Engineering, China, for two years. He joined the Department for Research and Development at Shanghai Xinhua Radio Factory, where he became a Senior Engineer and the Deputy Director of the Department in 1982. He performed research and design in the areas of microwave passive and active devices, receiver systems, PLL and AFC systems, and microwave integrated circuits. From June 1983 to September 1987, he was a Visiting Scientist with the Research Laboratory of Electronics, Massachusetts Institute of Technology. His research was on theoretical analyses of packaging and interconnection problems in ultrahigh-speed microelectronic integrated circuits. He joined the Shanghai Research Institute of Mechanical and Electrical Engineering, Shanghai, China, in October 1987. Since then, he has been a Professor and a Deputy Director of the Department of Electronic Engineering. He was engaged in development of a computer-based RF simulation system. In July 1989, he revisited the Research Laboratory of Electronics, MIT, where he is currently a Research Scientist. His research interests are in the areas of theory and experimentation of microwave systems and circuits; modeling and analysis of complex packaging problems in high-speed computers and microelectronic integrated circuits, and frequency-dependent nonlinear systems and circuits; RF simulation systems; and analysis and modeling of electromagnetic interferences. He has published two books, *Design of Microwave Integrated Circuits* and *Microwave Circuits Comprising Dielectric Resonators* in China, and over 40 journal articles.

Mr. Gu is a member of the Trustee Board of Shanghai Communication Association, China, and an Editor of the *Microwave Journal* published by the Chinese Institute of Electronics, China.

**Y. Eric Yang** was born in Taichung, Taiwan, on May 14, 1959. He received the B.S. degree from National Taiwan University, Taipei, Taiwan, in 1981, and the M.S., E.E., and Ph.D. degrees from the Massachusetts Institute of Technology, all in electrical engineering, in 1985, 1986, and 1989, respectively.

From 1981 to 1983 he was an Electronics Instructor of the R.O.C. Navy in Taiwan. While in graduate school, he was a Research Assistant and Teaching Assistant, and was engaged in the research area of electromagnetic modeling of microelectronic integrated circuits. He has been a Research Scientist in the Research Laboratory of Electronics at the Massachusetts Institute of Technology since 1989, conducting studies on electromagnetic interference and spectrum management, and radar imaging.

Dr. Yang was the recipient of an IBM Graduate Fellowship (1986–1987) and the URSI Henry George Booker Award for Young Scientist (1990). He is a member of Sigma Xi, Phi Tau Phi, and the Electromagnetics Academy.

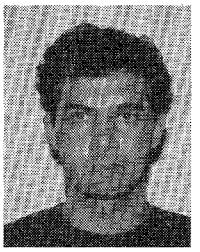

**M. Ali Tassoudji** (S'88) was born in Tehran, Iran, on February 4, 1965. He received the B.S. and M.S. degrees in electrical engineering from the University of Michigan, Ann Arbor, in 1987 and 1989, respectively.

He is now a Research Assistant at the Massachusetts Institute of Technology, where he is currently working toward his Ph.D. degree. His research interests include electromagnetic scattering and propagation, modeling of microwave circuits, and numerical techniques.